

# Crystal structure and magnetic properties of the spin- $\frac{1}{2}$ frustrated two-leg ladder compounds $(\text{C}_4\text{H}_{14}\text{N}_2)\text{Cu}_2\text{X}_6$ ( $X = \text{Cl}$ and $\text{Br}$ )

P. Biswal <sup>1,2,\*</sup>, S. Guchhait <sup>3,\*</sup>, S. Ghosh,<sup>4,\*</sup> S. N. Sarangi <sup>1</sup>, D. Samal,<sup>1,2</sup> Diptikanta Swain <sup>5,†</sup>, Manoranjan Kumar,<sup>4</sup> and R. Nath <sup>3,‡</sup>

<sup>1</sup>*Institute of Physics, Bhubaneswar 751005, India*

<sup>2</sup>*Homi Bhabha National Institute, Anushaktinagar, Mumbai 400094, India*

<sup>3</sup>*School of Physics, Indian Institute of Science Education and Research, Thiruvananthapuram-695551, Kerala, India*

<sup>4</sup>*Department of Condensed Matter and Materials Physics, S. N. Bose National Centre for Basic Sciences, Kolkata 700106, India*

<sup>5</sup>*Institute of Chemical Technology–IndianOil Odisha Campus, Bhubaneswar 751013, India*



(Received 27 June 2023; revised 14 August 2023; accepted 26 September 2023; published 16 October 2023)

We have successfully synthesized single crystals, solved the crystal structure, and studied the magnetic properties of a new family of copper halides  $(\text{C}_4\text{H}_{14}\text{N}_2)\text{Cu}_2\text{X}_6$  ( $X = \text{Cl}, \text{Br}$ ). These compounds crystallize in an orthorhombic crystal structure with space group  $Pnma$ . The crystal structure features  $\text{Cu}^{2+}$  dimers arranged parallel to each other that makes a zigzag two-leg ladderlike structure. Further, there exists a diagonal interaction between two adjacent dimers which generates interdimer frustration. Both the compounds manifest a singlet ground state with a large gap in the excitation spectrum. Magnetic susceptibility is analyzed in terms of both interacting spin- $\frac{1}{2}$  dimer and two-leg ladder models followed by exact diagonalization calculations. Our theoretical calculations in conjunction with the experimental magnetic susceptibility establish that the spin lattice can be described well by a frustrated two-leg ladder model with strong rung coupling [ $J_0/k_B = 116.0(2)$  and  $300.0(2)$  K], weak leg coupling [ $J'/k_B = 18.6(2)$  and  $105.0(2)$  K], and equally weak diagonal coupling [ $J''/k_B = 23.2(2)$  and  $90.0(2)$  K] for Cl and Br compounds, respectively. These exchange couplings set the critical fields very high, making them experimentally inaccessible. The correlation function decays exponentially as expected for a gapped spin system. The structural aspects of both the compounds are correlated with their magnetic properties. The calculation of entanglement witness divulges strong entanglement in both the compounds which persists up to high temperatures, even beyond 370 K for the Br compound.

DOI: [10.1103/PhysRevB.108.134420](https://doi.org/10.1103/PhysRevB.108.134420)

## I. INTRODUCTION

In recent days, the low-dimensional spin systems with singlet ground state are pursued rigorously as they manifest interesting field-induced quantum phases at low temperatures [1,2]. Moreover, the singlet state is considered to be a highly entangled state which has direct bearing on quantum computation and quantum communication [3–5]. The singlet ground state can be realized in the spin dimers [6], alternating spin chains [7,8], Haldane chains (integer spin chains) [9,10], spin-Peierls systems [11,12], even-leg ladders [13,14], frustrated magnets [15], etc.

An external magnetic field often acts as a perturbation, which continuously reduces the energy gap between the singlet ( $|S, S_z\rangle = |0, 0\rangle$ ) ground state and the triplet ( $|S, S_z\rangle = |1, 1\rangle$ ) excited states. Above a critical field ( $H_{c1}$ ) when the gap is closed, several intriguing field-induced quantum phenomena emerge. To name a few, Bose-Einstein condensation (BEC) of triplons in coupled dimer systems [2,16–20], Tomonaga-Luttinger liquid (TLL) in one-dimensional

spin chains and spin ladders [21–23], magnetization plateaus in interacting dimers [24–26], Wigner crystallization [27], etc., have been realized. The most intricate one being the Shastry-Sutherland lattice that consists of orthogonal dimers embedded in a square lattice. It has an exact dimer product ground state when the ratio between the inter- and intra-dimer couplings is sufficiently low [28]. Upon increasing this ratio, the system goes through a quantum phase transition to a plaquette singlet state followed by an antiferromagnetic phase [29]. Applying external field and pressure, one can tune the coupling ratio and hence observe a series of quantum phase transitions [30,31]. Indeed, the famous Shastry-Sutherland lattice compound  $\text{SrCu}_2(\text{BO}_3)_2$  featuring orthogonal  $\text{Cu}^{2+}$  dimers depicts quantized plateaus at  $\frac{1}{8}$ ,  $\frac{1}{4}$ , and  $\frac{1}{3}$  of the magnetization and Wigner crystallization of magnons [24,32–35]. These field-induced phases are also observed in several high spin compounds but the quantum effects are more predominant in systems with spin- $\frac{1}{2}$  [25,26]. Further, the isolated spin dimers with a significant intradimer coupling show a large spin gap, whereas the presence of interdimer couplings leads to a drastic reduction in the gap value, making the compounds suitable for high-field studies.

Unlike the transition metal oxides, the metal-organic compounds are more suitable for such studies as one can easily tune the interdimer and intradimer exchange

\*These authors contributed equally to this work.

†diptisscu@gmail.com

‡rnath@iisertvm.ac.in

couplings, spin gap, and the ground state properties by engineering the synthesis conditions and changing the ligand [19]. For instance, the isolated spin- $\frac{1}{2}$  dimers in the metal-organic compound  $\text{Cu}_2(\text{IPA})_2(\text{DMF})(\text{H}_2\text{O})$  result in a large spin gap of about  $\sim 414$  K [36] while isolated dimers in  $\text{Cu}_2\text{Mg}_2(\text{CO}_3)(\text{OH})_6\cdot 2\text{H}_2\text{O}$  provide a much reduced spin gap of around  $\sim 7$  K [37]. The hierarchy of the intradimer couplings depends on the interaction path involved, symmetry of the orbitals, bond length, bond angle, etc. Further, the interdimer coupling which significantly modifies the spin gap can be engineered by an appropriate choice of organic ligands [38–40]. Unfortunately, the database for organic coupled-dimer compounds with a spin gap is too small compared to the inorganic counterpart.  $[\text{Cu}_2(\text{apyhist})_2\text{Cl}_2](\text{ClO}_4)_2$ ,  $[\text{Cu}(\text{pyz})(\text{gly})](\text{ClO}_2)$ , and  $\text{NiCl}_2\cdot 4\text{SC}(\text{NH}_2)_2$  are a few examples of organic compounds reported with a small spin gap that show field-induced BEC physics [19,41,42].

In this paper, we report in detail the crystal growth, structure, and magnetic properties of two isostructural spin- $\frac{1}{2}$  strong rung coupled two-leg ladder compounds  $(\text{C}_4\text{H}_{14}\text{N}_2)\text{Cu}_2\text{X}_6$  ( $X = \text{Cl}$  and  $\text{Br}$ ) with a large spin gap. Our experimental magnetic susceptibility data are modeled well by the exact diagonalization (ED) calculations assuming a two-leg ladder model with a diagonal interaction that frustrates the spin lattice. It is found that the rung, leg, as well as the diagonal couplings for the Br compound are significantly larger as compared to the Cl compound [i.e.,  $J_0(\text{Br})/J_0(\text{Cl}) \sim 2.6$ ,  $J''(\text{Br})/J''(\text{Cl}) \sim 5.74$ , and  $J'(\text{Br})/J'(\text{Cl}) \sim 3.9$ ]. The relatively large exchange couplings in the case of the Br compound is attributed to its larger ionic size and more diffused  $p$  orbitals which increases the effective coupling between the  $\text{Cu}^{2+}$  ions. Our work provides a pathway to manipulate the magnetic properties of low-dimensional metal-organic compounds by judiciously changing the halide atom in the magnetically active network.

## II. TECHNIQUES

Single crystals of  $(\text{C}_4\text{H}_{14}\text{N}_2)\text{Cu}_2\text{Cl}_6$  and  $(\text{C}_4\text{H}_{14}\text{N}_2)\text{Cu}_2\text{Br}_6$  were prepared following the solution evaporation method by using a hot air oven in moderate temperatures. To synthesize  $(\text{C}_4\text{H}_{14}\text{N}_2)\text{Cu}_2\text{Cl}_6$ ,  $\text{C}_4\text{H}_{12}\text{N}_2$  ( $N, N'$ -Dimethylethylenediamine), and  $\text{CuCl}_2$  were added in molar ratio of 1:2 with little excess of  $\text{HCl}$ . Later, distilled water was added and the solution was heated at  $80^\circ\text{C}$  followed by continuous stirring for complete dissolution of the precursors. The resulting clear solution was kept inside an oven at  $45^\circ\text{C}$  which yielded greenish-yellow colored single crystals of  $(\text{C}_4\text{H}_{14}\text{N}_2)\text{Cu}_2\text{Cl}_6$  after 5 to 6 days. A similar procedure was followed to obtain single crystals of  $(\text{C}_4\text{H}_{14}\text{N}_2)\text{Cu}_2\text{Br}_6$  by taking the initial constituents  $\text{C}_4\text{H}_{12}\text{N}_2$ ,  $\text{CuBr}_2$ , and  $\text{HBr}$ . The only difference is that, the solution was heated at  $75^\circ\text{C}$  instead of  $45^\circ\text{C}$ , which resulted in dark-red colored needle-shaped crystals.

Single-crystal x-ray diffraction (XRD) was performed on good quality single crystals at room temperature using a Bruker KAPPA-II machine with a CCD detector and graphite monochromated  $\text{Mo } K\alpha$  radiation ( $\lambda_{\text{avg}} = 0.71073 \text{ \AA}$ ). The data were collected using APEX3 software and reduced with SAINT/XPREP [43]. An empirical absorption correction was

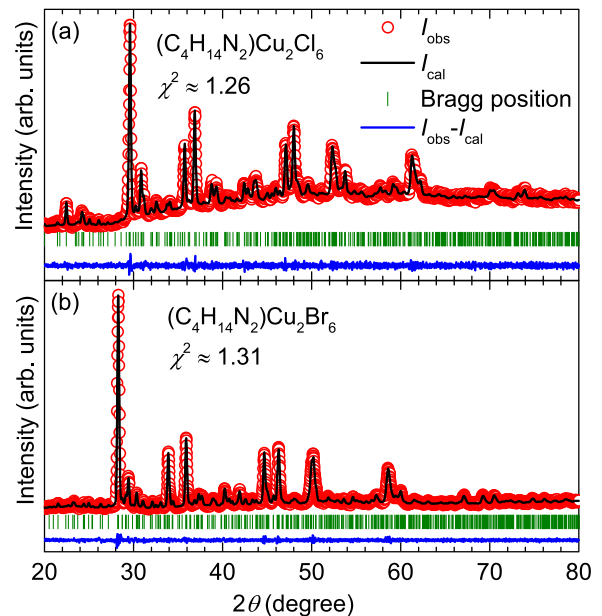


FIG. 1. Powder XRD patterns (open circles) at room temperature for (a)  $(\text{C}_4\text{H}_{14}\text{N}_2)\text{Cu}_2\text{Cl}_6$  and (b)  $(\text{C}_4\text{H}_{14}\text{N}_2)\text{Cu}_2\text{Br}_6$ . The solid line is the Le Bail fit of the data. The vertical bars indicate the expected Bragg peak positions and the bottom solid line corresponds to the difference between the observed and calculated intensities.

done using the SADABS program [44]. The structure was solved with direct methods using SHELXT-2018/2 [45] and refined by the full matrix least squares on  $F^2$  using SHELXL-2018/3, respectively [46]. All the hydrogen atoms were placed geometrically and held in the riding atom model for the final refinement. The final refinement included atomic positions for all the atoms, anisotropic thermal parameters for all the nonhydrogen atoms, and isotropic thermal parameters for the hydrogen atoms. The crystal data and detailed information about the structure refinement parameters are listed in Table I. To reconfirm the phase purity, a large number of single crystals were crushed into powder, and powder XRD measurement was performed at room temperature using a PANalytical ( $\text{Cu } K\alpha$  radiation,  $\lambda_{\text{avg}} = 1.5406 \text{ \AA}$ ) diffractometer. The powder XRD patterns were analyzed by Le Bail fit using the FULLPROF software package [47]. The initial structural parameters for the fits were taken from the single-crystal data (Table I). As shown in Fig. 1, all the peaks in the room temperature powder XRD pattern of both compounds could be indexed properly with orthorhombic structure ( $Pnma$ ). The refined lattice parameters and unit-cell volume are [ $a = 15.0583(10) \text{ \AA}$ ,  $b = 6.0273(5) \text{ \AA}$ ,  $c = 14.6121(7) \text{ \AA}$ , and  $V_{\text{cell}} \simeq 1326.22 \text{ \AA}^3$ ] and [ $a = 15.7969(11) \text{ \AA}$ ,  $b = 6.2901(3) \text{ \AA}$ ,  $c = 14.9536(9) \text{ \AA}$ , and  $V_{\text{cell}} \simeq 1485.87 \text{ \AA}^3$ ] for  $(\text{C}_4\text{H}_{14}\text{N}_2)\text{Cu}_2\text{Cl}_6$  and  $(\text{C}_4\text{H}_{14}\text{N}_2)\text{Cu}_2\text{Br}_6$ , respectively. These structural parameters of both the compounds are close to the single-crystal data.

Magnetization ( $M$ ) was measured using a superconducting quantum interference device (SQUID) magnetometer (MPMS, Quantum Design) in the temperature range  $2 \text{ K} \leq T \leq 350 \text{ K}$ , and in different applied fields ( $H$ ). Isothermal magnetization ( $M$  vs  $H$ ) measurement was performed at  $T = 2 \text{ K}$  varying the applied field from 0 to 5 T. For this purpose, a

TABLE I. Structure information of  $(C_4H_{14}N_2)Cu_2X_6$  ( $X = Cl, Br$ ) compounds obtained from the single-crystal XRD measurements at room temperature.

Crystal data		
Empirical formula	$(C_4H_{14}N_2)Cu_2Cl_6$	$(C_4H_{14}N_2)Cu_2Br_6$
Formula weight ( $M_r$ )	429.95 g/mole	696.71 g/mole
Crystal system	Orthorhombic	Orthorhombic
Space group	$Pnma$	$Pnma$
$a$ [Å]	15.040(1)	15.849(3)
$b$ [Å]	6.014(5)	6.3157(5)
$c$ [Å]	14.593(9)	14.992(3)
$V_{cell}$ [Å <sup>3</sup> ]	1319.95(17)	1500.6(5)
$Z$	4	4
Calculated crystal density ( $\rho_{cal}$ )	2.164 mg/mm <sup>3</sup>	3.084 mg/mm <sup>3</sup>
Absorption coefficient ( $\mu$ )	4.401 mm <sup>-1</sup>	18.780 mm <sup>-1</sup>
Crystal size	0.25 × 0.22 × 0.17 mm <sup>3</sup>	0.22 × 0.18 × 0.12 mm <sup>3</sup>
Data collection		
Temperature (K)	295(2)	295(2)
Radiation type	Mo $K\alpha$	Mo $K\alpha$
Wavelength ( $\lambda$ )	0.71073 Å	0.71073 Å
Diffractometer	Bruker KAPPA APEX-II CCD	Bruker KAPPA APEX-II CCD
$\theta$ range for data collection	2.708°–26.422°	2.570°–25.462°
Index ranges	$-18 \leq h \leq 18$ , $-7 \leq k \leq 7$ , $-18 \leq l \leq 18$	$-19 \leq h \leq 19$ , $-7 \leq k \leq 6$ , $-18 \leq l \leq 18$
$F(000)$	884	1280
Reflections collected	10316	11768
Independent reflections	1487 [ $R_{int} = 0.0462$ ]	1526 [ $R_{int} = 0.0685$ ]
Data/restraints/parameters	1487/0/85	1526/5/73
Final $R$ indexes, $I \geq 2\sigma(I)$	$R_1 = 0.0261$ , $\omega R_2 = 0.0549$	$R_1 = 0.1005$ , $\omega R_2 = 0.2441$
Final $R$ indexes, all data	$R_1 = 0.0389$ , $\omega R_2 = 0.0621$	$R_1 = 0.1346$ , $\omega R_2 = 0.2904$
Refinement		
Refinement method	Full-matrix least squares on $F^2$	Full-matrix least squares on $F^2$
Goodness-of-fit on $F^2$	1.123	1.017

large number of single crystals were crushed into powder and mounted on the sample rod.

Magnetization data were modeled by spin- $\frac{1}{2}$  interacting dimer and two-leg ladder models as well as via ED calculations. The ground state of interacting dimers, in general, has a short correlation length. Therefore, small system size ED calculations should be sufficient to obtain a reliable spectrum and thermodynamic properties. We employ the conventional ED method to obtain the full energy spectrum of the system size up to  $N = 24$  and found that  $N = 18$  is sufficient to reproduce the experimental magnetization data.

### III. RESULTS

#### A. Crystal structure

Both compounds are found to have the same crystal structure [orthorhombic,  $Pnma$  ( $D_{2h}^{16}$ , No. 62)] with  $Z = 4$ . The detailed crystallographic parameters obtained from the single-crystal XRD analysis such as lattice parameters ( $a$ ,  $b$ , and  $c$ ), unit-cell volume ( $V_{cell}$ ), etc., are summarized in Table I. The atomic positions, bond lengths, bond angles, and anisotropic atomic displacement parameters are tabulated in

the Supplemental Material (SM) [48]. The crystal structure obtained from the single-crystal XRD is presented in Fig. 2. The asymmetric unit of the crystal contains one  $N$ ,  $N'$ -Dimethylethylenediamonium ( $N$ ,  $N'$ D) cation and one  $Cu_2X_6$  ( $X = Cl, Br$ ) anion where both reside on mirror plane symmetry with an occupancy of 0.50. There are two inequivalent Cu sites and six inequivalent halide (Cl/Br) sites present in the crystal unit cell. Each Cu atom is coordinated with six halide (Cl/Br) atoms forming a distorted  $CuX_6$  octahedra. The octahedra are highly distorted with significant elongation of the Cu- $X$  bond along the apical direction. The calculated distortion parameters are given in the SM [48]. It is found that  $CuCl_6$  octahedra are more distorted compared to the  $CuBr_6$  one. In the basal plane, the Cu- $X$  bond distance for the Cl compound varies from 2.234 to 2.365 Å while the longest apical bond distances are in the range of 3.014 to 3.022 Å. Similarly, for the Br compound the bond distance in the basal plane varies from 2.39 Å to 2.43 Å while the apical bond distances are in the range of 3.163–3.17 Å.

Each structural dimer unit of  $Cu_2X_{10}$  is formed by edge sharing of two inequivalent  $CuX_6$  octahedra at the basal plane [see Fig. 2(b)]. Along the  $b$  direction, the dimers are arranged parallel to each other and are interconnected via the edge

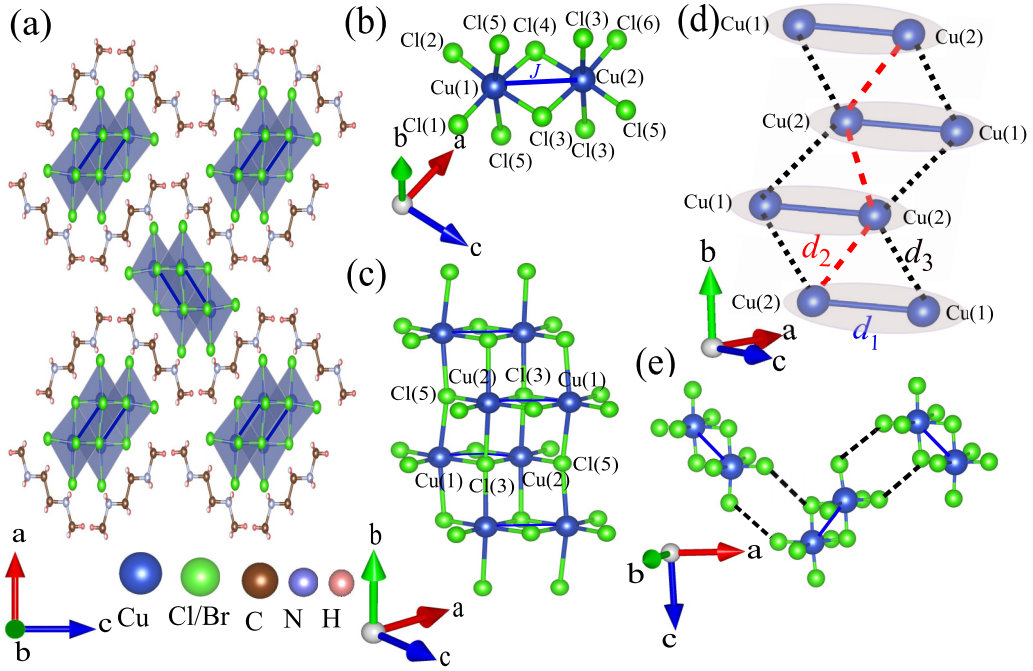


FIG. 2. (a) Three-dimensional view of the crystal structure of  $(\text{C}_4\text{H}_{14}\text{N}_2)\text{Cu}_2\text{X}_6$  ( $X = \text{Cl}, \text{Br}$ ) projected in the  $ac$  plane. (b) The  $\text{Cu}_2\text{X}_{10}$  ( $X = \text{Cl}, \text{Br}$ ) dimer unit with intradimer exchange coupling  $J_0$ . (c) Edge sharing of distorted  $\text{CuX}_6$  octahedra favoring interdimer couplings or couplings along the legs and diagonal of the ladder. (d) A sketch of the possible exchange couplings (after removing  $X$ ) highlight the coupled dimers or the frustrated two-leg zigzag ladder structure. (e) Orthogonal dimers from neighboring ladders.

sharing of  $\text{CuX}_6$  octahedra (between the apical and basal halide atoms) [see Fig. 2(c)]. In addition to the Cu-Cu intradimer distance  $d_1$ , if interdimer distance  $d_3$  is taken into account, the spin lattice would behave like a zigzag two-leg ladder structure with  $d_1$  and  $d_3$  representing the rungs and legs of the ladder, respectively. The diagonal distance  $d_2$  which is slightly less than  $d_3$  makes the spin lattice more intricate [see Fig. 2(d)]. These ladders are well apart and the organic cations reside in the interstitial space surrounding the ladders. Furthermore, the dimers from each ladder are aligned nearly perpendicular to the dimers of the neighboring ladders [see Fig. 2(e)]. The value of bond distances  $d_1$ ,  $d_2$ , and  $d_3$  and the corresponding angles  $\angle\text{Cu-X-Cu}$  that favor the interaction paths  $J_0$ ,  $J'$ , and  $J''$ , respectively, are tabulated in Table II.

## B. Magnetization

Figure 3 presents the temperature-dependent magnetic susceptibility ( $\chi \equiv M/H$ ) of  $(\text{C}_4\text{H}_{14}\text{N}_2)\text{Cu}_2\text{X}_6$  ( $X = \text{Cl}, \text{Br}$ ) measured in an applied field of  $\mu_0 H = 0.1$  T. Upon cooling,  $\chi(T)$  of both compounds shows a Curie-Weiss (CW) increase in the high-temperature regime and passes through a broad maxima at around  $T_\chi^{\text{max}} \simeq 72.5$  and 171.8 K, respectively, indicating the development of short-range antiferromagnetic (AFM) correlations. Below  $T_\chi^{\text{max}}$ ,  $\chi(T)$  of both compounds falls rapidly, which is a primary indication of the opening of a spin gap. At low temperatures, below 12.5 K (Cl) and 37.9 K (Br),  $\chi(T)$  of these systems increases due to the presence of a small fraction of extrinsic paramagnetic impurities or lattice imperfections in the samples. There is no signature of magnetic long-range order down to 2 K for both compounds.

TABLE II. Values of bond lengths  $d_1$ ,  $d_2$ , and  $d_3$  as shown in Fig. 2(d) and angles  $\angle\text{Cu-X-Cu}$  as shown in Figs. 2(b) and 2(c) for both the compounds corresponding to the exchange pathways  $J_0$ ,  $J'$ , and  $J''$ .

Compound	$J_0$		$J'$		$J''$	
	$d_1$ (Å)	Angle (deg)	$d_2$ (Å)	Angle (deg)	$d_3$ (Å)	Angle (deg)
$(\text{C}_4\text{H}_{14}\text{N}_2)\text{Cu}_2\text{Cl}_6$	3.4730	$\angle\text{Cu}(2)\text{-Cl}(3)\text{-Cu}(1)$	3.8809	$\angle\text{Cu}(2)\text{-Cl}(3)\text{-Cu}(2)$	3.933	$\angle\text{Cu}(1)\text{-Cl}(3)\text{-Cu}(2)$
		= 95.03		= 91.95		= 93.20
		$\angle\text{Cu}(2)\text{-Cl}(4)\text{-Cu}(1)$		$\angle\text{Cu}(1)\text{-Cl}(5)\text{-Cu}(2)$		
$(\text{C}_4\text{H}_{14}\text{N}_2)\text{Cu}_2\text{Br}_6$	3.650	= 98.84	4.070	$\angle\text{Cu}(2)\text{-Br}(4)\text{-Cu}(2)$	4.121	= 95.72
		$\angle\text{Cu}(2)\text{-Br}(3)\text{-Cu}(1)$		= 92.77		
		= 97.61		$\angle\text{Cu}(2)\text{-Br}(5)\text{-Cu}(1)$		= 94.95
		= 94.73				

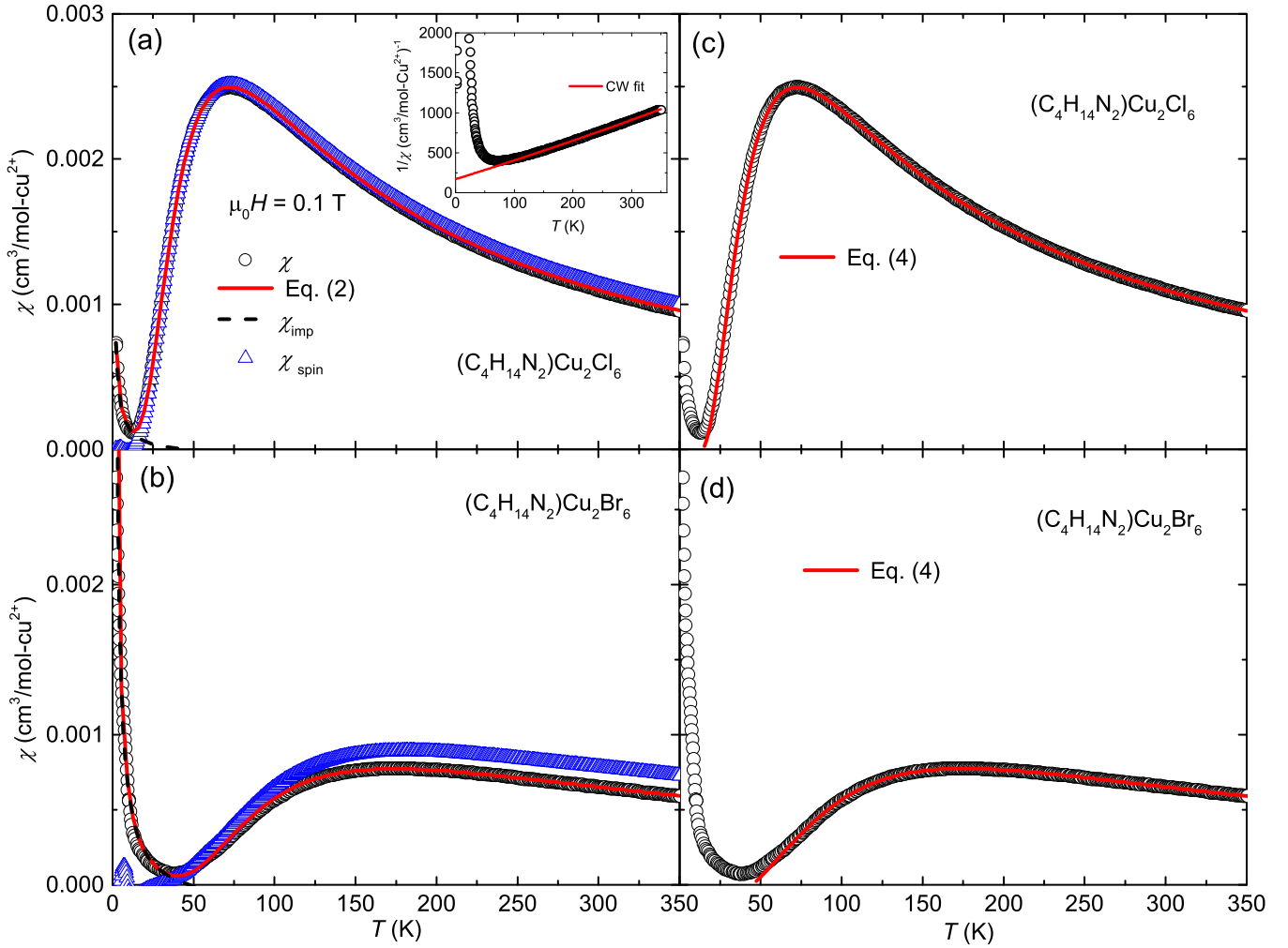


FIG. 3.  $\chi$  vs  $T$  in an applied field of  $\mu_0 H = 0.1$  T for (a)  $(\text{C}_4\text{H}_{14}\text{N}_2)\text{Cu}_2\text{Cl}_6$  and (b)  $(\text{C}_4\text{H}_{14}\text{N}_2)\text{Cu}_2\text{Br}_6$ . The solid line is the fit of the data using the spin- $\frac{1}{2}$  interacting-dimer model [Eq. (2)]. Inset:  $1/\chi$  vs  $T$  and the solid line is the CW fit for  $(\text{C}_4\text{H}_{14}\text{N}_2)\text{Cu}_2\text{Cl}_6$ .  $\chi$  vs  $T$  with isolated two-leg ladder model fit [Eq. (4)] for (c)  $(\text{C}_4\text{H}_{14}\text{N}_2)\text{Cu}_2\text{Cl}_6$  and (d)  $(\text{C}_4\text{H}_{14}\text{N}_2)\text{Cu}_2\text{Br}_6$ .

$\chi(T)$  at high temperatures was fitted by the sum of CW law and the temperature-independent susceptibility ( $\chi_0$ ):

$$\chi(T) = \chi_0 + \frac{C}{T - \theta_{\text{CW}}}. \quad (1)$$

Here,  $C$  and  $\theta_{\text{CW}}$  are the Curie constant and CW temperature, respectively. The inverse susceptibility [ $1/\chi(T)$ ] of  $(\text{C}_4\text{H}_{14}\text{N}_2)\text{Cu}_2\text{Cl}_6$  was fitted above 200 K by Eq. (1) that yields  $\chi_0 \simeq -1.08 \times 10^{-4}$   $\text{cm}^3/\text{mol-Cu}^{2+}$ ,  $C \simeq 0.45$   $\text{cm}^3 \text{K}/\text{mol-Cu}^{2+}$ , and  $\theta_{\text{CW}} \simeq -75$  K. The negative value of  $\theta_{\text{CW}}$  indicates a dominant AFM interaction between the  $\text{Cu}^{2+}$  ions. The effective magnetic moment estimated from the  $C$  value to be  $\mu_{\text{eff}} = (3k_{\text{B}}C/N_{\text{A}}\mu_{\text{B}}^2)^{1/2} \simeq 1.89\mu_{\text{B}}/\text{Cu}^{2+}$  (where  $k_{\text{B}}$  is the Boltzmann constant,  $N_{\text{A}}$  is the Avogadro's number, and  $\mu_{\text{B}}$  is the Bohr magneton). This value of  $\mu_{\text{eff}}$  is slightly higher than the free ion value of  $\mu_{\text{eff}}$  ( $1.73\mu_{\text{B}}$ ) for  $\text{Cu}^{2+}$  with spin- $\frac{1}{2}$  and  $g = 2$ . The  $\mu_{\text{eff}}$  value corresponds to  $g \simeq 2.18$ , typically observed for  $\text{Cu}^{2+}$ -based systems [49,50]. As the exchange coupling for  $(\text{C}_4\text{H}_{14}\text{N}_2)\text{Cu}_2\text{Br}_6$  is relatively large and our  $\chi(T)$  measurements are restricted to 350 K only, it was not possible to fit the data using Eq. (1). This is because, CW fit requires data at very large temperatures  $T > \theta_{\text{CW}}$  [51]

and measurement above 350 K was not possible since both the compounds melt at around 420 K (see SM [48]). To understand the exchange network,  $\chi(T)$  data over the whole temperature range were fitted by the equation

$$\chi(T) = \chi_0 + \frac{C_{\text{imp}}}{T - \theta_{\text{imp}}} + \chi_{\text{spin}}(T). \quad (2)$$

In the second term,  $C_{\text{imp}}$  is the Curie constant of the impurity spins and  $\theta_{\text{imp}}$  is the effective interaction strength between the impurity spins. This term takes care of the low-temperature Curie tail in  $\chi(T)$ .  $\chi_{\text{spin}}(T)$  is the spin susceptibility of the spin- $\frac{1}{2}$  interacting dimer model which has the form [40]

$$\chi_{\text{spin}}(T) = \frac{N_{\text{A}}g^2\mu_{\text{B}}^2}{k_{\text{B}}T} \frac{1}{\left[3 + e^{(J_0/k_{\text{B}}T)} + \frac{z'J'}{k_{\text{B}}T}\right]}. \quad (3)$$

Here,  $J_0$  and  $J'$  are the intra- and average inter-dimer interactions, respectively. In this expression, a mean-field approximation is used to introduce  $J'$  in the isolated dimer model [36]. Here,  $z' = 2$  represents the number of neighboring dimers coupled with one dimer through  $J'$ . As shown in Fig. 3, Eq. (2) reproduces our experimental

data very well resulting in the parameters [ $\chi_0 \simeq -4.52 \times 10^{-5} \text{ cm}^3/\text{mol-Cu}^{2+}$ ,  $C_{\text{imp}} \simeq 0.002 \text{ cm}^3 \text{ K}/\text{mol-Cu}^{2+}$ ,  $\theta_{\text{imp}} \simeq -0.64 \text{ K}$ ,  $g = 2.05$ ,  $J_0/k_B = 116.7(6) \text{ K}$ , and  $J'/k_B = 25(1) \text{ K}$ ] and [ $\chi_0 \simeq -1.55 \times 10^{-4} \text{ cm}^3/\text{mol-Cu}^{2+}$ ,  $C_{\text{imp}} \simeq 0.00725 \text{ cm}^3 \text{ K}/\text{mol-Cu}^{2+}$ ,  $\theta_{\text{imp}} \simeq 0.53 \text{ K}$ ,  $g = 2.12$ ,  $J_0/k_B = 288.8(9) \text{ K}$ , and  $J'/k_B = 235(1) \text{ K}$ ] for  $(\text{C}_4\text{H}_{14}\text{N}_2)\text{Cu}_2\text{Cl}_6$  and  $(\text{C}_4\text{H}_{14}\text{N}_2)\text{Cu}_2\text{Br}_6$ , respectively. The obtained values of  $C_{\text{imp}}$  correspond to  $\sim 0.53\%$  and  $\sim 1.9\%$  of the paramagnetic impurity spins, respectively, assuming spin  $\frac{1}{2}$ . In order to emphasize the gapped behavior,  $\chi_0 + \frac{C_{\text{imp}}}{T - \theta_{\text{imp}}}$  was subtracted from the  $\chi(T)$  data. The resulting intrinsic  $\chi_{\text{spin}}(T)$  indeed decays exponentially towards zero at low temperatures [see Figs. 3(a) and 3(b)], further establishing a singlet ground state. For  $T < 12 \text{ K}$  (in the gapped state),  $\chi_{\text{spin}}$  of the Br compound [see Fig. 3(b)] shows an anomalous feature which is likely due to unreliable subtraction of the extrinsic contributions.

As demonstrated in Fig. 2(d), there is equal possibility for the parallel dimers to interact along the legs of the ladder. Therefore, we fitted the  $\chi(T)$  data by the high- $T$  series expansion (HTSE) of the strong rung ladder model as

$$\chi(T) = \chi_0 + \chi_{\text{spin}}(T). \quad (4)$$

Here,  $\chi_{\text{spin}}$  is the expression of HTSE for the spin- $\frac{1}{2}$  two-leg ladder with strong rung coupling [i.e., Eq. (47) in Ref. [52]]. This expression is valid in high temperatures and for  $0 \leq J''/J_0 \leq 1$ . This expression predicts more accurate results for  $J''/J_0 < 0.6$ . Our fit in the high- $T$  regime  $T > 0.2J_0$  (i.e., 25 K for Cl and 68 K for Br) reproduces the experimental data very well yielding [ $\chi_0 \simeq -4.99 \times 10^{-5} \text{ cm}^3/\text{mol-Cu}^{2+}$ ,  $g \simeq 2.06$ ,  $J_0/k_B = 115(1) \text{ K}$ , and  $J''/k_B = 23(1) \text{ K}$ ] and [ $\chi_0 \simeq -1.108 \times 10^{-4} \text{ cm}^3/\text{mol-Cu}^{2+}$ ,  $g \simeq 2.06$ ,  $J_0/k_B = 271(1) \text{ K}$ , and  $J''/k_B = 99.6(7) \text{ K}$ ] for Cl and Br compounds, respectively [see Figs. 3(c) and 3(d)].

The zero-field spin gap ( $\Delta_0$ ) for a strong rung coupled two-leg ladder can be estimated as [52]

$$\Delta_0 = J_0 - J'' + \frac{J''^2}{2J_0} + \frac{J''^3}{4J_0^2} - \frac{J''^4}{8J_0^3} + \mathcal{O}(J''^5). \quad (5)$$

Using the appropriate values of  $J_0$  and  $J''$ ,  $\Delta_0$  is calculated to be 94.7 and 192.3 K for the Cl and Br compounds, respectively. The values of spin gap correspond to the critical field of gap closing  $\mu_0 H_{C1} \simeq 68.4 \text{ T}$  and 146.4 T for the Cl and Br compounds, respectively. Similarly, the saturation field ( $H_{C2}$ ) at which one can achieve the fully polarized state is calculated to be  $\mu_0 H_{C2} = (J_0 + 2J'')/g\mu_B \simeq 115 \text{ T}$  and 358 T for the Cl and Br compounds, respectively [13]. Magnetic isotherm ( $M$  vs  $H$ ) measured at  $T = 2 \text{ K}$  is shown in Fig. 4. For both the compounds, it shows a typical paramagnetic behavior up to 5 T. The  $\chi(T)$  analysis suggests that  $\chi_{\text{spin}}(T)$  approaches zero value below  $\sim 13$  and  $\sim 37 \text{ K}$  for  $(\text{C}_4\text{H}_{14}\text{N}_2)\text{Cu}_2\text{Cl}_6$  and  $(\text{C}_4\text{H}_{14}\text{N}_2)\text{Cu}_2\text{Br}_6$ , respectively, and the low- $T$  upturn in  $\chi(T)$  is entirely due to extrinsic contributions. As one expects zero magnetization in the gapped state, the observed  $M$  vs  $H$  behavior can be attributed completely due to the paramagnetic impurity spins. Hence, one can estimate this extrinsic paramagnetic contribution accurately by fitting the data to [53]

$$M(H) = \chi H + f_{\text{imp}} N_A g_{\text{imp}} \mu_B S_{\text{imp}} B_{S_{\text{imp}}}(x). \quad (6)$$

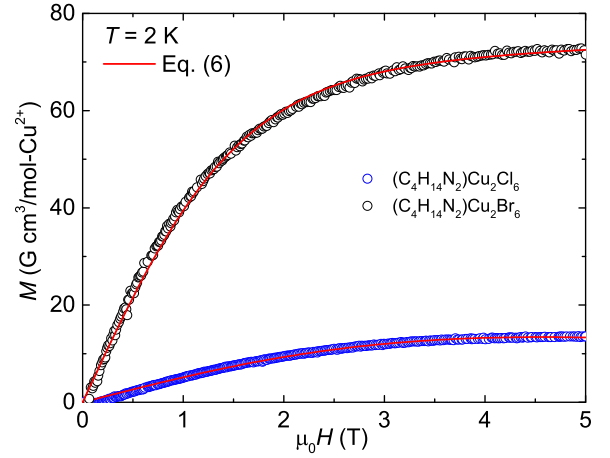


FIG. 4. Magnetization isotherms ( $M$  vs  $H$ ) at  $T = 2 \text{ K}$  measured up to 5 T. Solid lines are the Brillouin fit using Eq. (6).

In the above equation,  $\chi$  is the intrinsic susceptibility,  $f_{\text{imp}}$  is the molar fraction of the impurities,  $g_{\text{imp}}$  is the impurity  $g$  factor,  $S_{\text{imp}}$  is the impurity spin,  $B_{S_{\text{imp}}}(x)$  is the Brillouin function, and  $x = g_{\text{imp}} \mu_B S_{\text{imp}} H / [k_B (T - \theta_{\text{imp}})]$ . We assumed the impurity spin  $S_{\text{imp}} = \frac{1}{2}$  and the Brillouin function reduces to  $B_{S_{\text{imp}}}(x) = \tanh(x)$  [54]. Our fitted results upon fixing  $g = 2$  are ( $f_{\text{imp}} \simeq 0.0048 \text{ mol } \%$  and  $\theta_{\text{imp}} \simeq -0.44 \text{ K}$ ) and ( $f_{\text{imp}} \simeq 0.0122 \text{ mol } \%$  and  $\theta_{\text{imp}} \simeq 0.95 \text{ K}$ ) for the Cl and Br compounds, respectively. The obtained values of  $f_{\text{imp}}$  correspond to  $\sim 0.48\%$  and  $\sim 1.2\%$  of spin- $\frac{1}{2}$  paramagnetic impurity spins for the Cl and Br compounds, respectively, which are consistent with the  $\chi(T)$  analysis.

### C. Quantum entanglement

The existence of entanglement in an AFM spin system can be measured by a quantity called entanglement witness (EW). In a magnetic system with singlet ground state, the two spins are strongly entangled and one can extract EW from the macroscopic thermodynamic observable like  $\chi_{\text{spin}}$ . For a spin- $\frac{1}{2}$  isotropic Heisenberg system, EW is related to  $\chi_{\text{spin}}$  as [55]

$$\text{EW} = 1 - \frac{6k_B T \chi_{\text{spin}}}{N_A g^2 \mu_B^2}. \quad (7)$$

Figure 5 depicts the temperature variation of EW calculated using Eq. (7). The EW of both compounds reaches a maximum value of 1 in the low-temperature region where  $\chi_{\text{spin}}$  is zero. It decreases with increasing temperature. For  $(\text{C}_4\text{H}_{14}\text{N}_2)\text{Cu}_2\text{Cl}_6$ , EW approaches zero at around 120 K, whereas for  $(\text{C}_4\text{H}_{14}\text{N}_2)\text{Cu}_2\text{Br}_6$ , it remains nonzero even at 370 K. For an entangled state, EW should have a finite value ( $> 0$ ). The dashed line [Eq. (7) taking EW = 0] in the insets of Figs. 5(a) and 5(b) represents the boundary of the entangled state, which is plotted along with  $\chi_{\text{spin}}(T)$ . The point of intersection with  $\chi_{\text{spin}}$  defines the upper temperature limit of the entangled state. The dashed curve intersects the  $\chi_{\text{spin}}$  data of  $(\text{C}_4\text{H}_{14}\text{N}_2)\text{Cu}_2\text{Cl}_6$  at around 120 K, which is consistent with the above analysis. On the other hand,  $(\text{C}_4\text{H}_{14}\text{N}_2)\text{Cu}_2\text{Br}_6$  demonstrates that entanglement persists even beyond 370 K. Experimentally, quantum entanglement is realized in several

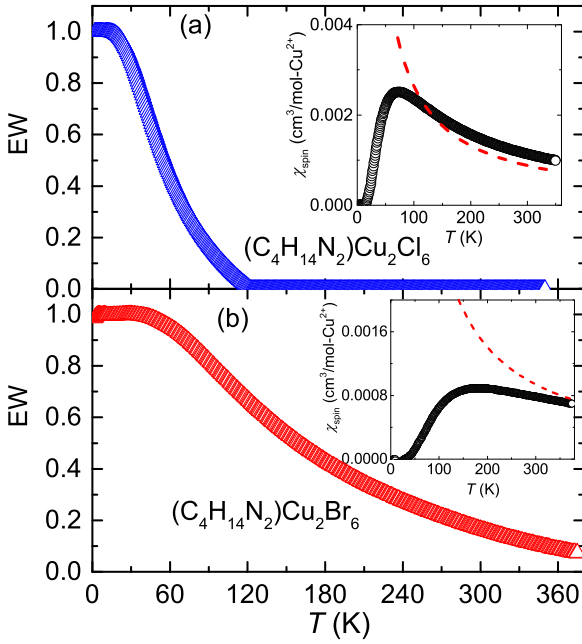


FIG. 5. Entanglement witness (EW) as a function of temperature for (a)  $(\text{C}_4\text{H}_{14}\text{N}_2)\text{Cu}_2\text{Cl}_6$  and (b)  $(\text{C}_4\text{H}_{14}\text{N}_2)\text{Cu}_2\text{Br}_6$ . Inset:  $\chi_{\text{spin}}$  vs  $T$  along with the entanglement boundary (dashed line).

spin- $\frac{1}{2}$  Heisenberg AFM dimers and spin-chain systems such as  $\text{Cu}(\text{NO}_3)_2 \cdot 2.5\text{H}_2\text{O}$  [56],  $\text{Na}_2\text{Cu}_5\text{Si}_4\text{O}_{14}$  [57],  $\text{NH}_4\text{CuPO}_4 \cdot \text{H}_2\text{O}$  [58], and  $\text{Cu}(\text{tz})_2\text{Cl}_2$  [59]. However, all these compounds are entangled at very low temperatures except  $\text{Na}_2\text{Cu}_5\text{Si}_4\text{O}_{14}$ . In this context,  $(\text{C}_4\text{H}_{14}\text{N}_2)\text{Cu}_2\text{Cl}_6$  and  $(\text{C}_4\text{H}_{14}\text{N}_2)\text{Cu}_2\text{Br}_6$  are two promising compounds where entanglement perseveres up to much higher temperatures compared to the above-mentioned compounds.

#### D. Theoretical calculations

A frustrated two-leg ladder is pictorially shown in Fig. 6, where each solid sphere represents a  $\text{Cu}^{2+}$  site with spin- $\frac{1}{2}$ . The two inequivalent Cu sites are denoted as A and B. An isotropic spin- $\frac{1}{2}$  Heisenberg model Hamiltonian on this lattice can be written as

$$\begin{aligned} \mathcal{H} = & \sum_{i=1}^{N/2} J_0 \vec{S}_{i,A} \cdot \vec{S}_{i,B} + \sum_{i=1}^{N/2} J' \vec{S}_{i,B} \cdot \vec{S}_{i+1,B} \\ & + \sum_{i=1}^{N/2} J'' (\vec{S}_{i,B} \cdot \vec{S}_{i+1,A} + \vec{S}_{i,A} \cdot \vec{S}_{i+1,B}) \\ & - H \sum_{i=1}^{N/2} (S_{i,A}^z + S_{i,B}^z), \end{aligned} \quad (8)$$

where  $\vec{S}_{i,A}$  and  $\vec{S}_{i,B}$  indicate the spin vectors for the sublattices A and B, respectively, of the  $i$ th unit cell. In Eq. (8), the first term represents the intradimer coupling  $J_0$  while the second and third terms represent the interdimer coupling  $J'$  and  $J''$  between the neighboring dimers along the diagonal and the leg, respectively. The coupling  $J'$  is always between two same Cu sites while  $J''$  is between two inequivalent Cu sites. The last term of the Hamiltonian represents an externally applied

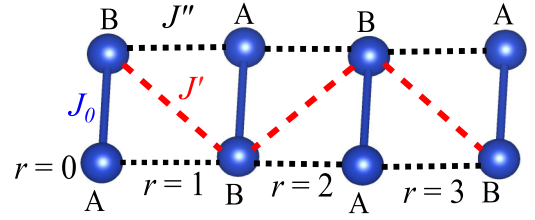


FIG. 6. Lattice structure: A and B are two sublattices of the ladder structure.  $J_0$  and  $J''$  are rung and leg couplings, respectively, while  $J'$  is the coupling along the diagonal.  $r$  is the site index along the lower leg of the system.

axial magnetic field  $H$ , and the energy scale is set in terms of  $J_0$ .

In order to have further insight into the ground state properties, correlation function,  $C(r) = \langle \Psi | S_i \cdot S_{i+r} | \Psi \rangle$  vs distance  $r$  of the lattice sites, and magnetization  $M = \langle \psi | \sum_{i=1}^N s_i^z | \psi \rangle$  vs magnetic field ( $H$ ), calculations are performed up to  $N = 24$  sites by considering the frustrated two-leg ladder model. The magnetization  $M(T, H)$  and magnetic susceptibility  $\chi(T, H)$  of these systems can be calculated using the full spectrum and the partition function  $Z(T, H)$  can be written as

$$Z(T, H) = \sum_{s^z = -N/2}^{N/2} \sum_{n_{s^z}} e^{-\beta(E_{n_{s^z}} - H s^z)}. \quad (9)$$

Here,  $\beta = \frac{1}{k_B T}$  and  $s^z$  is the  $z$  component of total spin which varies from  $-N/2$  to  $N/2$  where the total number of sites in the system is  $N$ .  $E_{n_{s^z}}$  is the energy for the  $n_{s^z}$  state. The magnetization can be defined as

$$M(T, H) = \frac{1}{N} \sum_{s^z = -N/2}^{N/2} \sum_{n_{s^z}} s^z e^{-\beta(E_{n_{s^z}} - H s^z)}. \quad (10)$$

$\chi(T, H)$  can be written in terms of the magnetic fluctuation as

$$\chi(T, H) = \frac{\beta}{N} [\langle M^2 \rangle - \langle M \rangle^2]. \quad (11)$$

First, we calculated the magnetic susceptibility  $\chi(T)$  by taking the frustrated two-leg ladder model into account for both materials. As the experimental  $\chi(T)$  contains a large low-temperature upturn (see Fig. 3), to fit the experimental data, we used the spin susceptibility  $\chi_{\text{spin}}$  originating from the interacting dimer model fit in Fig. 3. In order to show the finite-size effect,  $\chi_{\text{spin}}$  is calculated for three different system sizes,  $N = 12, 16,$  and  $18$ . Clearly, there is no visible finite-size effect for both compounds. From the best fit of the experimental  $\chi_{\text{spin}}$  data in Fig. 7, the obtained parameters are [ $g = 2.06$ ,  $J_0/k_B = 116.0(2)$  K,  $J'/k_B = 23.2(2)$  K, and  $J''/k_B = 18.6(2)$  K] for  $(\text{C}_4\text{H}_{14}\text{N}_2)\text{Cu}_2\text{Cl}_6$  and [ $g = 2.06$ ,  $J_0/k_B = 300.0(2)$  K,  $J'/k_B = 90.0(2)$  K, and  $J''/k_B = 105.0(2)$  K] for  $(\text{C}_4\text{H}_{14}\text{N}_2)\text{Cu}_2\text{Br}_6$ , respectively. We also calculated the correlation function  $C(r)$  for the frustrated two-leg ladder model for both compounds along the A-B-A-B-... sites (see Fig. 6), where  $r$  is the distance. We notice that  $C(r)$  decays exponentially along the leg (A-B-A-B-...) and it can be fitted well with an exponential function  $Ae^{-r/\xi}$  where  $A$  is a constant. From the fit in Fig. 8, the correlation length  $\xi$  is estimated to be  $\sim 0.36$  and  $\sim 0.64$  for  $(\text{C}_4\text{H}_{14}\text{N}_2)\text{Cu}_2\text{Cl}_6$  and

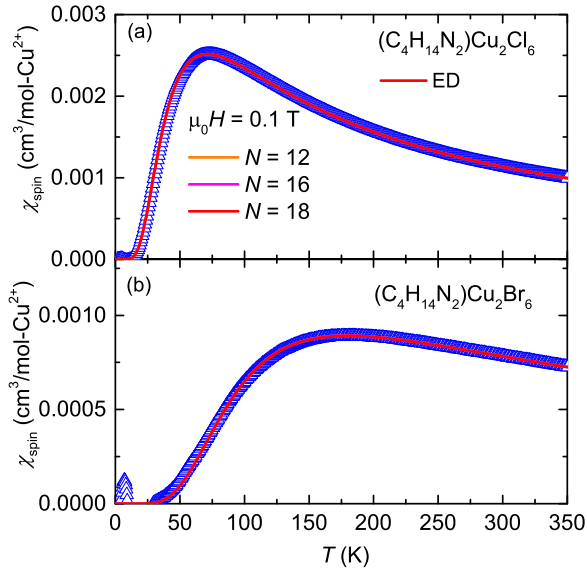


FIG. 7. The experimental  $\chi_{\text{spin}}$  data (symbols) for (a)  $(\text{C}_4\text{H}_{14}\text{N}_2)\text{Cu}_2\text{Cl}_6$  and (b)  $(\text{C}_4\text{H}_{14}\text{N}_2)\text{Cu}_2\text{Br}_6$ . The fits using ED simulation for the frustrated two-leg ladder are shown as solid lines for system sizes  $N = 12, 16,$  and  $18$ .

$(\text{C}_4\text{H}_{14}\text{N}_2)\text{Cu}_2\text{Br}_6$ , respectively, which are still less than the spacing between nearest-neighbor  $\text{Cu}^{2+}$  ions along the leg. Surprisingly, for  $(\text{C}_4\text{H}_{14}\text{N}_2)\text{Cu}_2\text{Br}_6$ , despite large  $J'/J_0$  and  $J''/J_0$  ratios ( $\sim 0.30$  and  $0.35$ ),  $\xi$  is less than the lattice spacing and it is still behaving like weakly coupled dimers.

The spin gap and saturation field are two important quantities to understand the magnetic properties of a gapped spin system. Due to large energy scale of the exchange couplings, the critical fields are too high and are not accessible experimentally. Hence, to extract the value of critical fields (critical field of gap closing  $H_{C1}$  and saturation field  $H_{C2}$ ) and to understand the nature of magnetic isotherms, we have simulated the  $M$  vs  $H$  curve at zero temperature for both compounds for  $N = 20$  and  $24$  sites (see Fig. 9). The critical fields are

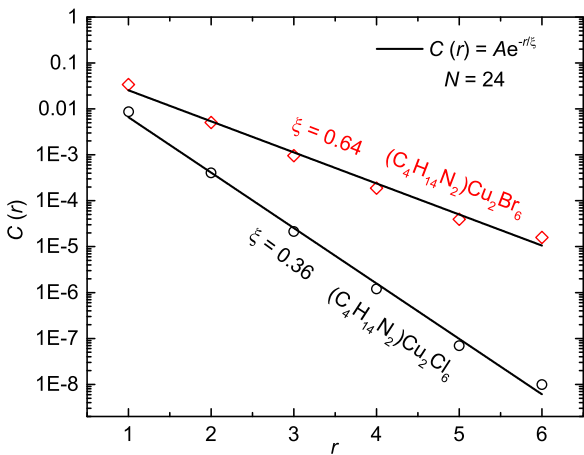


FIG. 8. The correlation function  $C(r)$  vs  $r$  calculated for the frustrated two-leg ladder model along the lower leg by taking  $r = 0$  as the reference site (see Fig. 6) for  $(\text{C}_4\text{H}_{14}\text{N}_2)\text{Cu}_2\text{Cl}_6$  and  $(\text{C}_4\text{H}_{14}\text{N}_2)\text{Cu}_2\text{Br}_6$ . Solid lines are the exponential fits.

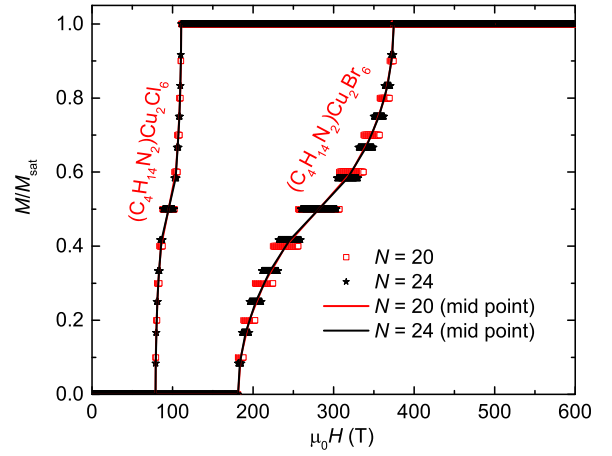


FIG. 9. The calculated  $M$  vs  $H$  curves for  $(\text{C}_4\text{H}_{14}\text{N}_2)\text{Cu}_2\text{Cl}_6$  and  $(\text{C}_4\text{H}_{14}\text{N}_2)\text{Cu}_2\text{Br}_6$  with system sizes  $N = 20$  and  $24$  using the frustrated two-leg ladder model. Symbols and solid lines represent the plateaus and connector of the midpoint of plateaus, respectively.

found to be independent of the system size for both the compounds. In the intermediate field regime, the Cl compound has very weak finite-size effect while the Br compound exhibits a plateaulike behavior and should have a continuous  $M$  vs  $H$  curve in the thermodynamic limit ( $N \rightarrow \infty$ ). Finite-size effects can be avoided by considering the value of  $M$  at the midpoint of each plateau and drawing a continuous line through these points for  $N = 20$  and  $24$  which show almost no difference. The value of  $\mu_0 H_{C1}$  is found to be  $78.9$  and  $181.2$  T for the Cl and Br compounds, respectively. This suggests that such a robust singlet ground state cannot be perturbed by the experimentally available magnetic fields. The saturation magnetic field or the field required to obtain the fully polarized state is found to be  $\mu_0 H_{C2} = 110.7$  T and  $374.2$  T for the Cl and Br compounds, respectively. These values of  $H_{C1}$  and  $H_{C2}$  are slightly larger than the ones predicted from the analysis using the two-leg ladder model, as the two-leg ladder model does not take into account the diagonal interaction.

#### IV. DISCUSSION AND SUMMARY

We investigated the structural and magnetic properties of two copper halides. Although experimental  $\chi(T)$  data are fitted well by both spin- $\frac{1}{2}$  interacting dimer and two-leg ladder models, a more accurate description is obtained from the ED calculations. The ED calculation results assuming a two-leg ladder model reproduce the spin susceptibility more precisely with a strong rung coupling  $J_0/k_B = 116.0(2)$  and  $300.0(2)$  K, a weak but significant leg coupling  $J''/k_B = 18.6(2)$  and  $105.0(2)$  K, and another weak diagonal coupling  $J'/k_B = 23.2(2)$  and  $90.0(2)$  K for  $(\text{C}_4\text{H}_{14}\text{N}_2)\text{Cu}_2\text{Cl}_6$  and  $(\text{C}_4\text{H}_{14}\text{N}_2)\text{Cu}_2\text{Br}_6$ , respectively. Depending on the hierarchy of the exchange couplings, two-leg spin- $\frac{1}{2}$  ladders may evince remarkable critical behavior at low temperatures due to low dimensionality and reduced spin value. For instance, although TLL physics is envisaged in two-leg ladders, a qualitative difference is delineated between strong-leg and strong-rung ladders. Theory predicts attractive fermionic interaction in strong-leg spin- $\frac{1}{2}$  ladders [e.g.,  $(\text{C}_7\text{H}_{10}\text{N})_2\text{CuBr}_4$ ] and

repulsive fermionic interaction in strong-rung spin- $\frac{1}{2}$  ladders [e.g.,  $(\text{C}_5\text{H}_{12}\text{N})_2\text{CuBr}_4$ ], respectively, in the gapless TLL critical state [22,23]. Similarly, spin- $\frac{1}{2}$  two-leg ladders above  $H_{C1}$ , are also foretold to feature a dimensional crossover from a one-dimensional TLL state at high temperatures to a three-dimensional BEC state at low temperatures, as observed in  $(\text{C}_5\text{H}_{12}\text{N})_2\text{CuBr}_4$ ,  $(\text{C}_7\text{H}_{10}\text{N})_2\text{CuBr}_4$ , and  $(\text{C}_5\text{H}_{12}\text{N})_2\text{CuCl}_4$  [23,60,61]. Experimental verification of such predictions is strongly hindered as the number of two-leg ladder compounds are limited to date [13,60–68]. Thus, because of the two-leg ladder structure, the compounds under investigation have the potential to host these quantum phases, if the values of exchange couplings can be lowered significantly. Further, as depicted in Fig. 6, the AFM  $J'$  along the diagonal induces magnetic frustration in the ladder, making it a unique spin lattice of frustrated two-leg ladder in both our compounds [69].

According to the Goodenough-Kanamori-Anderson (GKA) rule, the nature and strength of the superexchange in magnetic insulators depend very much on the Cu- $X$ -Cu bridging angle and the extent of overlap between the Cu  $3d$  and  $X$   $3p/4p$  orbitals of the ligands ( $X = \text{Cl}, \text{Br}$ ). Strong AFM exchange interaction is favored for  $\angle\text{Cu-}X\text{-Cu} > 95^\circ$  [70]. As discussed earlier, the  $\text{CuX}_6$  octahedra are distorted due to the Jahn-Teller effect and the Cu- $X$  bond is elongated along the apical direction. In an octahedral coordination, the  $3d_{x^2-y^2}$  orbital of  $\text{Cu}^{2+}$  lies in the basal plane and contains the unpaired electron. In both the compounds, the intradimer (or rung) coupling ( $J_0$ ) arises due to the overlapping of  $3d_{x^2-y^2}$  orbitals of two  $\text{Cu}^{2+}$  ions via the quasiorthogonal  $p$  orbitals of the halide ligands in the basal plane. On the other hand, the diagonal ( $J'$ ) and leg ( $J''$ ) interactions emerge from the overlapping of  $3d_{z^2}$  orbitals of one  $\text{Cu}^{2+}$  with  $3d_{x^2-y^2}$  orbitals of another  $\text{Cu}^{2+}$  from the neighboring dimers via the  $p$  orbitals of the apical halide ions of the distorted  $\text{CuX}_6$  octahedra. Furthermore, the intradimer distance  $d_1$  is found to be smaller than  $d_2$  and  $d_3$  and the angle  $\angle\text{Cu-}X\text{-Cu}$  along  $d_2$  and  $d_3$  (see Table II). Thus, the presence of an unpaired electron in the  $3d_{x^2-y^2}$  orbital, shorter bond distance, and larger bond angle are the obvious reasons for much stronger AFM coupling for  $J_0$  as compared to  $J'$  and  $J''$ . Due to the extended Cu- $X$ - $X$ -Cu paths, the orthogonal dimers of the neighboring ladders are very weakly connected in the  $ac$  plane through the basal halide ions. The magnetic network of these compounds seems to be similar to the celebrated compounds  $\text{ACuX}_3$  ( $A = \text{Ti}, \text{NH}_4, \text{K}$ ) [71].

Despite the same crystal structure, the exchange couplings ( $J_0$ ,  $J'$ , and  $J''$ ) of  $(\text{C}_4\text{H}_{14}\text{N}_2)\text{Cu}_2\text{Br}_6$  are larger than  $(\text{C}_4\text{H}_{14}\text{N}_2)\text{Cu}_2\text{Cl}_6$ . The Cu-Cu bond distance and  $\angle\text{Cu-}X\text{-Cu}$  bond angles (see Table II) for both the compounds are nearly the same and making a distinction is really difficult. The superexchange mechanism between  $\text{Cu}^{2+}$  ions is explained well for  $\text{CuX}_2$  ( $X = \text{F}, \text{Cl}, \text{and Br}$ ) in Ref. [72] in terms of the GKA rule [70]. It is reported that the larger ligand size can amplify the orbital overlap mechanism, leading to larger exchange couplings. Since  $\text{Br}^-$  has a larger ionic radius than  $\text{Cl}^-$ , one expects higher  $J_0$ ,  $J'$ , and  $J''$  for  $(\text{C}_4\text{H}_{14}\text{N}_2)\text{Cu}_2\text{Br}_6$  than  $(\text{C}_4\text{H}_{14}\text{N}_2)\text{Cu}_2\text{Cl}_6$ . Similar results are reported for the alternating chain compound,  $(4, 4'\text{-bipyridinium})\text{Cu}_2\text{Cl}_{6-x}\text{Br}_x$ , where the AFM couplings are increased monotonously with

increasing bromide concentration [73]. Moreover, distortion in the  $\text{CuX}_6$  octahedra units also plays a decisive role. In the case of  $\text{CuCl}_6$ , the distortion is more than  $\text{CuBr}_6$  which possibly favors weaker interaction in  $(\text{C}_4\text{H}_{14}\text{N}_2)\text{Cu}_2\text{Cl}_6$ .

For an isolated dimer compound, the intradimer coupling represents the true spin gap in zero field and the critical field of gap closing ( $H_{C1}$ ) coincides with the critical field of saturation ( $H_{C2}$ ). The interdimer coupling not only reduces the value of spin gap but also increases the spread between  $H_{C1}$  and  $H_{C2}$ , allowing space for field-induced quantum phases to occur [1,16]. As shown in Fig. 9, these fields are  $\mu_0 H_{C1} \simeq 78.9$  T and  $\mu_0 H_{C2} \simeq 110.7$  T for the Cl compound and  $\mu_0 H_{C1} \simeq 181.2$  T and  $\mu_0 H_{C2} \simeq 374.2$  T for the Br compound. Thus, the large spacing between  $H_{C1}$  and  $H_{C2}$  implies significant interdimer coupling or leg coupling along the ladder for both the compounds, consistent with our  $\chi(T)$  analysis. Unfortunately, their exchange couplings are so large that the critical fields are not easily accessible experimentally. However, the exchange couplings in these compounds can be reduced by appropriately choosing the halide ions and ligands or introducing more distortion in the lattice. Another interesting aspect of these compounds is that the dimers from one ladder are nearly orthogonal to the dimers in the neighboring ladders. Therefore, if the interdimer couplings can be weakened by tuning structural parameters, then these compounds can be considered equivalent to the Shastry-Sutherland lattices  $\text{Sr}_2\text{Cu}(\text{BO}_3)_2$  and  $\text{BaNd}_2\text{ZnO}_5$  [24,74]. Thus, synthesis of these compounds opens up a new route to tune the magnetic parameters and realize new compounds that would be relevant from the quantum magnetism point of view.

In summary, we present the details of single-crystal growth and magnetic properties of two interesting isostructural quantum magnets  $(\text{C}_4\text{H}_{14}\text{N}_2)\text{Cu}_2\text{X}_6$  ( $X = \text{Cl}, \text{Br}$ ). Both the compounds feature  $\text{Cu}^{2+}$  two-leg ladders with a frustrated diagonal coupling. The dimers from each ladder are aligned orthogonal to the dimers from the adjacent ladders. The analysis of  $\chi(T)$  and the subsequent theoretical calculations reveal that the dimers are strongly coupled leading to a drastic reduction in spin gap from its isolated dimer value. Our exact diagonalization calculations assuming a frustrated two-leg ladder geometry, indeed, reproduce the experimental  $\chi(T)$  with leading rung coupling  $J_0/k_B = 116.0(2)$  and  $300.0(2)$  K, weak leg coupling  $J'/k_B = 18.6(2)$  and  $105.0(2)$  K, and weak frustrated diagonal coupling  $J''/k_B = 23.2(2)$  and  $90.0(2)$  K for the Cl and Br compounds, respectively. Despite same crystal symmetry, the relatively large exchange couplings in the case of Br as compared to the Cl compound is attributed to the larger ionic size of  $\text{Br}^-$  and more diffused  $p$  orbitals that facilitate stronger coupling between the  $\text{Cu}^{2+}$  ions. Further tuning of exchange couplings by appropriately choosing the halide ions or ligands would make them model compounds for exploring field-induced quantum phases.

## ACKNOWLEDGMENTS

S. Guchhait and R. Nath acknowledge SERB, India for financial support bearing Sanction Grant No. CRG/2022/000997. S. Guchhait is supported by the Prime Minister's Research Fellowship (PMRF) scheme, Govern-

ment of India. M.K. thanks SERB for financial support through Grant Sanction No. CRG/2020/000754. S.G. would like to express sincere gratitude to the DST-Inspire for finan-

cial support. D.S. acknowledges financial support from the Max Planck partner group and SERB, India (research Grant No. CRG/2019/005144).

- [1] T. Giamarchi, C. Rüegg, and O. Tchernyshyov, Bose–Einstein condensation in magnetic insulators, *Nat. Phys.* **4**, 198 (2008).
- [2] V. Zapf, M. Jaime, and C. D. Batista, “Bose-Einstein condensation in quantum magnets,” *Rev. Mod. Phys.* **86**, 563 (2014).
- [3] K. M. O’Connor and W. K. Wootters, Entangled rings, *Phys. Rev. A* **63**, 052302 (2001).
- [4] V. Vedral, Quantifying entanglement in macroscopic systems, *Nature (London)* **453**, 1004 (2008).
- [5] W. K. Wootters, Entanglement of formation of an arbitrary state of two qubits, *Phys. Rev. Lett.* **80**, 2245 (1998).
- [6] M. Kofu, J.-H. Kim, S. Ji, S.-H. Lee, H. Ueda, Y. Qiu, H.-J. Kang, M. A. Green, and Y. Ueda, Weakly coupled  $S = 1/2$  quantum spin singlets in  $\text{Ba}_3\text{Cr}_2\text{O}_8$ , *Phys. Rev. Lett.* **102**, 037206 (2009).
- [7] P. K. Mukharjee, K. M. Ranjith, M. Baenitz, Y. Skourski, A. A. Tsirlin, and R. Nath, Two types of alternating spin- $\frac{1}{2}$  chains and their field-induced transitions in  $\epsilon\text{-LiVOPO}_4$ , *Phys. Rev. B* **101**, 224403 (2020).
- [8] P. K. Mukharjee, K. M. Ranjith, B. Koo, J. Sichelschmidt, M. Baenitz, Y. Skourski, Y. Inagaki, Y. Furukawa, A. A. Tsirlin, and R. Nath, Bose-Einstein condensation of triplons close to the quantum critical point in the quasi-one-dimensional spin- $\frac{1}{2}$  antiferromagnet  $\text{NaVOPO}_4$ , *Phys. Rev. B* **100**, 144433 (2019).
- [9] Y. Uchiyama, Y. Sasago, I. Tsukada, K. Uchinokura, A. Zheludev, T. Hayashi, N. Miura, and P. Böni, Spin-vacancy-induced long-range order in a new Haldane-gap antiferromagnet, *Phys. Rev. Lett.* **83**, 632 (1999).
- [10] T. Shimizu, D. E. MacLaughlin, P. C. Hammel, J. D. Thompson, and S.-W. Cheong, Spin susceptibility and low-lying excitations in the Haldane-gap compound  $\text{Y}_2\text{BaNiO}_5$ , *Phys. Rev. B* **52**, R9835 (1995).
- [11] M. Hase, I. Terasaki, and K. Uchinokura, Observation of the spin-Peierls transition in linear  $\text{Cu}^{2+}$  (spin- $1/2$ ) chains in an inorganic compound  $\text{CuGeO}_3$ , *Phys. Rev. Lett.* **70**, 3651 (1993).
- [12] S. K. Saha, M. S. Roy, M. Kumar, and Z. G. Soos, Modeling the spin-Peierls transition of spin- $\frac{1}{2}$  chains with correlated states:  $J_1\text{-}J_2$  model,  $\text{CuGeO}_3$ , and  $\text{TTF-CuS}_4\text{C}_4(\text{CF}_3)_4$ , *Phys. Rev. B* **101**, 054411 (2020).
- [13] C. P. Landee, M. M. Turnbull, C. Galeriu, J. Giantsidis, and F. M. Woodward, Magnetic properties of a molecular-based spin-ladder system:  $(\text{5IAP})_2\text{CuBr}_4 \cdot 2\text{H}_2\text{O}$ , *Phys. Rev. B* **63**, 100402(R) (2001).
- [14] M. Azuma, Z. Hiroi, M. Takano, K. Ishida, and Y. Kitaoka, Observation of a spin-gap in  $\text{SrCu}_2\text{O}_3$  comprising spin- $\frac{1}{2}$  quasi-1D two-leg ladders, *Phys. Rev. Lett.* **73**, 3463 (1994).
- [15] R. Budnik and A. Auerbach, Low-energy singlets in the Heisenberg antiferromagnet on the kagome lattice, *Phys. Rev. Lett.* **93**, 187205 (2004).
- [16] C. Rüegg, N. Cavadini, A. Furrer, H.-U. Güdel, K. Krämer, H. Mutka, A. Wildes, K. Habicht, and P. Vorderwisch, Bose–Einstein condensation of the triplet states in the magnetic insulator  $\text{TlCuCl}_3$ , *Nature (London)* **423**, 62 (2003).
- [17] A. A. Aczel, Y. Kohama, C. Marcenat, F. Weickert, M. Jaime, O. E. Ayala-Valenzuela, R. D. McDonald, S. D. Selesnic, H. A. Dabkowska, and G. M. Luke, Field-induced Bose-Einstein condensation of triplons up to 8 K in  $\text{Sr}_3\text{Cr}_2\text{O}_8$ , *Phys. Rev. Lett.* **103**, 207203 (2009).
- [18] C. Rüegg, D. F. McMorrow, B. Normand, H. M. Rønnow, S. E. Sebastian, I. R. Fisher, C. D. Batista, S. N. Gvasaliya, C. Niedermayer, and J. Stahn, Multiple magnon modes and consequences for the Bose-Einstein condensed phase in  $\text{BaCuSi}_2\text{O}_6$ , *Phys. Rev. Lett.* **98**, 017202 (2007).
- [19] R. S. Freitas, W. A. Alves, and A. Paduan-Filho, Magnetic-field-induced ordered phase in the chloro-bridged copper(II) dimer system  $[\text{Cu}_2(\text{apyhist})_2\text{Cl}_2](\text{ClO}_4)_2$ , *Phys. Rev. B* **95**, 184426 (2017).
- [20] G. Hester, H. S. Nair, T. Reeder, D. R. Yahne, T. N. DeLazzer, L. Berges, D. Ziat, J. R. Neilson, A. A. Aczel, G. Sala, J. A. Quilliam, and K. A. Ross, Novel strongly spin-orbit coupled quantum dimer magnet:  $\text{Yb}_2\text{Si}_2\text{O}_7$ , *Phys. Rev. Lett.* **123**, 027201 (2019).
- [21] M. Ozerov, M. Maksymenko, J. Wosnitza, A. Honecker, C. P. Landee, M. M. Turnbull, S. C. Furuya, T. Giamarchi, and S. A. Zvyagin, Electron spin resonance modes in a strong-leg ladder in the Tomonaga-Luttinger liquid phase, *Phys. Rev. B* **92**, 241113(R) (2015).
- [22] M. Jeong, D. Schmidiger, H. Mayaffre, M. Klanjšek, C. Berthier, W. Knafo, G. Ballon, B. Vignolle, S. Krämer, A. Zheludev, and M. Horvatić, Dichotomy between attractive and repulsive Tomonaga-Luttinger liquids in spin ladders, *Phys. Rev. Lett.* **117**, 106402 (2016).
- [23] M. Jeong, H. Mayaffre, C. Berthier, D. Schmidiger, A. Zheludev, and M. Horvatić, Attractive Tomonaga-Luttinger liquid in a quantum spin ladder, *Phys. Rev. Lett.* **111**, 106404 (2013).
- [24] H. Kageyama, K. Yoshimura, R. Stern, N. V. Mushnikov, K. Onizuka, M. Kato, K. Kosuge, C. P. Slichter, T. Goto, and Y. Ueda, Exact dimer ground state and quantized magnetization plateaus in the two-dimensional spin system  $\text{SrCu}_2(\text{BO}_3)_2$ , *Phys. Rev. Lett.* **82**, 3168 (1999).
- [25] G. S. Murugan, K. R. Babu, R. Sankar, W. T. Chen, I. P. Muthuselvam, S. Chattopadhyay, and K.-Y. Choi, Magnetic and structural dimer networks in layered  $\text{K}_2\text{Ni}(\text{MoO}_4)_2$ , *Phys. Rev. B* **103**, 024451 (2021).
- [26] M. Uchida, H. Tanaka, H. Mitamura, F. Ishikawa, and T. Goto, High-field magnetization process in the  $S = 1$  quantum spin system  $\text{Ba}_3\text{Mn}_2\text{O}_8$ , *Phys. Rev. B* **66**, 054429 (2002).
- [27] P. Horsch, M. Sofin, M. Mayr, and M. Jansen, Wigner crystallization in  $\text{Na}_3\text{Cu}_2\text{O}_4$  and  $\text{Na}_8\text{Cu}_5\text{O}_{10}$  chain compounds, *Phys. Rev. Lett.* **94**, 076403 (2005).
- [28] B. S. Shastry and B. Sutherland, Exact ground state of a quantum mechanical antiferromagnet, *Physica B+C* **108**, 1069 (1981).
- [29] A. Koga and N. Kawakami, Quantum phase transitions in the Shastry-Sutherland model for  $\text{SrCu}_2(\text{BO}_3)_2$ , *Phys. Rev. Lett.* **84**, 4461 (2000).

- [30] M. E. Zayed, C. Rüegg, J. Larrea J., A. M. Läuchli, C. Panagopoulos, S. S. Saxena, M. Ellerby, D. F. McMorrow, T. Strässle, S. Klotz, G. Hamel, R. A. Sadykov, V. Pomjakushin, M. Boehm, M. Jiménez-Ruiz, A. Schneidewind, E. Pomjakushina, M. Stingaciu, K. Conder, and H. M. Rønnow, 4-spin plaquette singlet state in the Shastry–Sutherland compound  $\text{SrCu}_2(\text{BO}_3)_2$ , *Nat. Phys.* **13**, 962 (2017).
- [31] M. Takigawa, M. Horvatić, T. Waki, S. Krämer, C. Berthier, F. Lévy-Bertrand, I. Sheikin, H. Kageyama, Y. Ueda, and F. Mila, Incomplete devil's staircase in the magnetization curve of  $\text{SrCu}_2(\text{BO}_3)_2$ , *Phys. Rev. Lett.* **110**, 067210 (2013).
- [32] S. Miyahara and K. Ueda, Exact dimer ground state of the two dimensional Heisenberg spin system  $\text{SrCu}_2(\text{BO}_3)_2$ , *Phys. Rev. Lett.* **82**, 3701 (1999).
- [33] K. Onizuka, H. Kageyama, Y. Narumi, K. Kindo, Y. Ueda, and T. Goto,  $1/3$  magnetization plateau in  $\text{SrCu}_2(\text{BO}_3)_2$ -stripe order of excited triplets, *J. Phys. Soc. Jpn.* **69**, 1016 (2000).
- [34] S. Haravifard, D. Graf, A. E. Feiguin, C. D. Batista, J. C. Lang, D. M. Silevitch, G. Srajer, B. D. Gaulin, H. A. Dabkowska, and T. F. Rosenbaum, Crystallization of spin superlattices with pressure and field in the layered magnet  $\text{SrCu}_2(\text{BO}_3)_2$ , *Nat. Commun.* **7**, 11956 (2016).
- [35] K. Kodama, M. Takigawa, M. Horvatic, C. Berthier, H. Kageyama, Y. Ueda, S. Miyahara, F. Becca, and F. Mila, Magnetic superstructure in the two-dimensional quantum antiferromagnet  $\text{SrCu}_2(\text{BO}_3)_2$ , *Science* **298**, 395 (2002).
- [36] S. Thamban, U. Arjun, M. Padmanabhan, and R. Nath, Structural and magnetic properties of spin-1/2 dimer compound  $\text{Cu}_2(\text{IPA})_2(\text{DMF})(\text{H}_2\text{O})$  with a large spin gap, *J. Phys.: Condens. Matter* **29**, 255801 (2017).
- [37] S. Lebernegg, A. A. Tsirlin, O. Janson, and H. Rosner, Nearly compensated exchange in the dimer compound callaghanite  $\text{Cu}_2\text{Mg}_2(\text{CO}_3)(\text{OH})_6 \cdot 2\text{H}_2\text{O}$ , *Phys. Rev. B* **89**, 165127 (2014).
- [38] D. A. Tennant, S. E. Nagler, A. W. Garrett, T. Barnes, and C. C. Torardi, Excitation spectrum and superexchange pathways in the spin dimer  $\text{VODPO}_4 \cdot \frac{1}{2}\text{D}_2\text{O}$ , *Phys. Rev. Lett.* **78**, 4998 (1997).
- [39] J. W. Johnson, D. C. Johnston, A. J. Jacobson, and J. F. Brody, Preparation and characterization of vanadyl hydrogen phosphate hemihydrate and its topotactic transformation to vanadyl pyrophosphate, *J. Am. Chem. Soc.* **106**, 8123 (1984).
- [40] U. Arjun, V. Kumar, P. K. Anjana, A. Thirumurugan, J. Sichelschmidt, A. V. Mahajan, and R. Nath, Singlet ground state in the spin- $\frac{1}{2}$  weakly coupled dimer compound  $\text{NH}_4[(\text{V}_2\text{O}_3)_2(4, 4'-bpy)_2(\text{H}_2\text{PO}_4)(\text{PO}_4)_2] \cdot 0.5\text{H}_2\text{O}$ , *Phys. Rev. B* **95**, 174421 (2017).
- [41] O. Chiatti, A. Sytcheva, J. Wosnitza, S. Zherlitsyn, A. A. Zvyagin, V. S. Zapf, M. Jaime, and A. Paduan-Filho, Character of magnetic excitations in a quasi-one-dimensional antiferromagnet near the quantum critical points: Impact on magnetoacoustic properties, *Phys. Rev. B* **78**, 094406 (2008).
- [42] T. Lancaster, P. A. Goddard, S. J. Blundell, F. R. Foronda, S. Ghannadzadeh, J. S. Möller, P. J. Baker, F. L. Pratt, C. Baines, L. Huang, J. Wosnitza, R. D. McDonald, K. A. Modic, J. Singleton, C. V. Topping, T. A. W. Beale, F. Xiao, J. A. Schlueter, A. M. Barton, R. D. Cabrera *et al.*, Controlling magnetic order and quantum disorder in molecule-based magnets, *Phys. Rev. Lett.* **112**, 207201 (2014).
- [43] A. Bruker, APEX3, SAINT-Plus, XPREP, 2016.
- [44] G. M. Sheldrick, Siemens area correction absorption correction program, University of Göttingen, Göttingen, Germany (1994).
- [45] G. M. Sheldrick, SHELXT—Integrated space-group and crystal-structure determination, *Acta Crystallogr. A: Found. Adv.* **71**, 3 (2015).
- [46] G. M. Sheldrick, Shelxl-2018/3 software package, University of Göttingen, Germany (2018).
- [47] J. Rodríguez-Carvajal, Recent advances in magnetic structure determination by neutron powder diffraction, *Phys. B: Condens. Matter* **192**, 55 (1993).
- [48] See Supplemental Material at <http://link.aps.org/supplemental/10.1103/PhysRevB.108.134420> for additional information, which includes Ref. [75].
- [49] R. Nath, K. M. Ranjith, J. Sichelschmidt, M. Baenitz, Y. Skourski, F. Alet, I. Rousochatzakis, and A. A. Tsirlin, Hindered magnetic order from mixed dimensionalities in  $\text{CuP}_2\text{O}_6$ , *Phys. Rev. B* **89**, 014407 (2014).
- [50] X. P. Jin, Z. W. Ouyang, X. C. Liu, T. T. Xiao, J. J. Cao, Z. X. Wang, Z. C. Xia, and W. Tong, Two-sublattice description of the dimer-trimer chain compound  $\text{Li}_2\text{Cu}_5\text{Si}_4\text{O}_{14}$ : High-field magnetization and ESR studies, *Phys. Rev. B* **104**, 174423 (2021).
- [51] K. Somesh, Y. Furukawa, G. Simutis, F. Bert, M. Prinz-Zwick, N. Büttgen, A. Zorko, A. A. Tsirlin, P. Mendels, and R. Nath, Universal fluctuating regime in triangular chromate antiferromagnets, *Phys. Rev. B* **104**, 104422 (2021).
- [52] D. C. Johnston, M. Troyer, S. Miyahara, D. Lidsky, K. Ueda, M. Azuma, Z. Hiroi, M. Takano, M. Isobe, Y. Ueda, M. A. Korotin, V. I. Anisimov, A. V. Mahajan, and L. L. Miller, Magnetic susceptibilities of spin-1/2 antiferromagnetic Heisenberg ladders and applications to ladder oxide compounds, [arXiv:cond-mat/0001147](https://arxiv.org/abs/cond-mat/0001147).
- [53] R. Nath, Y. Singh, and D. C. Johnston, Magnetic, thermal, and transport properties of layered arsenides  $\text{BaRu}_2\text{As}_2$  and  $\text{SrRu}_2\text{As}_2$ , *Phys. Rev. B* **79**, 174513 (2009).
- [54] C. Kittel, *Introduction to Solid State Physics*, 8th ed. (Wiley, New York, 1986).
- [55] M. Wieśniak, V. Vedral, and Č. Brukner, Magnetic susceptibility as a macroscopic entanglement witness, *New J. Phys.* **7**, 258 (2005).
- [56] H. Singh, T. Chakraborty, P. K. Panigrahi, and C. Mitra, Experimental estimation of discord in an antiferromagnetic Heisenberg compound  $\text{Cu}(\text{NO}_3)_2 \cdot 2.5\text{H}_2\text{O}$ , *Quantum Inf. Process* **14**, 951 (2015).
- [57] A. M. Souza, M. S. Reis, D. O. Soares-Pinto, I. S. Oliveira, and R. S. Sarthour, Experimental determination of thermal entanglement in spin clusters using magnetic susceptibility measurements, *Phys. Rev. B* **77**, 104402 (2008).
- [58] T. Chakraborty, H. Singh, and C. Mitra, Signature of quantum entanglement in  $\text{NH}_4\text{CuPO}_4\text{H}_2\text{O}$ , *J. Appl. Phys.* **115**, 034909 (2014).
- [59] T. Chakraborty, H. Singh, D. Das, T. K. Sen, and C. Mitra, Quantification of entanglement from magnetic susceptibility for a Heisenberg spin 1/2 system, *Phys. Lett. A* **376**, 2967 (2012).
- [60] H. Ryll, K. Kiefer, C. Rüegg, S. Ward, K. W. Krämer, D. Biner, P. Bouillot, E. Coira, T. Giamarchi, and C. Kollath, Magnetic entropy landscape and Grüneisen parameter of a quantum spin ladder, *Phys. Rev. B* **89**, 144416 (2014).
- [61] M. Klanjšek, H. Mayaffre, C. Berthier, M. Horvatić, B. Chiari, O. Piovesana, P. Bouillot, C. Kollath, E. Orignac, R. Citro,

- and T. Giamarchi, Controlling Luttinger liquid physics in spin ladders under a magnetic field, *Phys. Rev. Lett.* **101**, 137207 (2008).
- [62] B. C. Watson, V. N. Kotov, M. W. Meisel, D. W. Hall, G. E. Granroth, W. T. Montfrooij, S. E. Nagler, D. A. Jensen, R. Backov, M. A. Petruska, G. E. Fanucci, and D. R. Talham, Magnetic spin ladder  $(\text{C}_5\text{H}_{12}\text{N})_2\text{CuBr}_4$ : High-field magnetization and scaling near quantum criticality, *Phys. Rev. Lett.* **86**, 5168 (2001).
- [63] H. Deguchi, S. Sumoto, S. Yamamoto, S. Takagi, H. Nojiri, and M. Motokawa, Magnetic properties of a Heisenberg spin-ladder  $\text{Cu}_2(\text{C}_5\text{H}_{12}\text{N}_2)_2\text{Br}_4$ , *Physica B: Condens. Matter* **284-288**, 1599 (2000).
- [64] G. Chaboussant, M.-H. Julien, Y. Fagot-Revurat, L. P. Lévy, C. Berthier, M. Horvatić, and O. Piovesana, Identification of nuclear relaxation processes in a gapped quantum magnet:  $^1\text{H}$  NMR in the  $S = \frac{1}{2}$  Heisenberg ladder  $\text{Cu}_2(\text{C}_5\text{H}_{12}\text{N}_2)_2\text{Cl}_4$ , *Phys. Rev. Lett.* **79**, 925 (1997); G. Chaboussant, P. A. Crowell, L. P. Lévy, O. Piovesana, A. Madouri, and D. Mailly, Experimental phase diagram of  $\text{Cu}_2(\text{C}_5\text{H}_{12}\text{N}_2)_2\text{Cl}_4$ : A quasi-one-dimensional antiferromagnetic spin- $\frac{1}{2}$  Heisenberg ladder, *Phys. Rev. B* **55**, 3046 (1997).
- [65] T. Imai, K. R. Thurber, K. M. Shen, A. W. Hunt, and F. C. Chou,  $^{17}\text{O}$  and  $^{63}\text{Cu}$  NMR in undoped and hole doped  $\text{Cu}_2\text{O}_3$  two-leg spin ladder  $A_{14}\text{Cu}_{24}\text{O}_{41}$  ( $A_{14} = \text{La}_6\text{Ca}_8, \text{Sr}_{14}, \text{Sr}_{11}\text{Ca}_3$ ), *Phys. Rev. Lett.* **81**, 220 (1998).
- [66] T. Hong, T. Ying, Q. Huang, S. E. Dissanayake, Y. Qiu, M. M. Turnbull, A. A. Podlesnyak, Y. Wu, H. Cao, Y. Liu, I. Umehara, J. Gouchi, Y. Uwatoko, M. Matsuda, D. A. Tennant, G.-W. Chern, K. P. Schmidt, and S. Wessel, Evidence for pressure induced unconventional quantum criticality in the coupled spin ladder antiferromagnet  $\text{C}_9\text{H}_{18}\text{N}_2\text{CuBr}_4$ , *Nat. Commun.* **13**, 3073 (2022).
- [67] T. Tajiri, H. Deguchi, M. Mito, S. Takagi, H. Nojiri, T. Kawae, and K. Takeda, Magnetic properties of isostructural spin-ladder systems  $(\text{C}_5\text{H}_{12}\text{N})_2\text{CuCl}_4$  and  $(\text{C}_5\text{H}_{12}\text{N})_2\text{CuCl}_2\text{Br}_2$ , *J. Magn. Magn. Mater.* **272-276**, 1070 (2004).
- [68] Z. Y. Zhao, B. Tong, X. Zhao, L. M. Chen, J. Shi, F. B. Zhang, J. D. Song, S. J. Li, J. C. Wu, H. S. Xu, X. G. Liu, and X. F. Sun, Thermal conductivity of  $\text{IPA-CuCl}_3$ : Evidence for ballistic magnon transport and the limited applicability of the Bose-Einstein condensation model, *Phys. Rev. B* **91**, 134420 (2015).
- [69] A. A. Tsirlin, I. Rousochatzakis, D. Kasinathan, O. Janson, R. Nath, F. Weickert, C. Geibel, A. M. Läuchli, and H. Rosner, Bridging frustrated-spin-chain and spin-ladder physics: Quasi-one-dimensional magnetism of  $\text{BiCu}_2\text{PO}_6$ , *Phys. Rev. B* **82**, 144426 (2010).
- [70] J. B. Goodenough, Theory of the role of covalence in the perovskite-type manganites  $[\text{La}, M(\text{II})]\text{MnO}_3$ , *Phys. Rev.* **100**, 564 (1955); J. Kanamori, Superexchange interaction and symmetry properties of electron orbitals, *J. Phys. Chem. Solids* **10**, 87 (1959); P. W. Anderson, Theory of magnetic exchange interactions: Exchange in insulators and semiconductors, *Solid State Phys.* **14**, 99 (1963).
- [71] M. Matsumoto, B. Normand, T. M. Rice, and M. Sigrist, Field- and pressure-induced magnetic quantum phase transitions in  $\text{TiCuCl}_3$ , *Phys. Rev. B* **69**, 054423 (2004).
- [72] S. Lebernegg, M. Schmitt, A. A. Tsirlin, O. Janson, and H. Rosner, Magnetism of  $\text{CuX}_2$  frustrated chains ( $X = \text{F}, \text{Cl}, \text{Br}$ ): Role of covalency, *Phys. Rev. B* **87**, 155111 (2013).
- [73] R. D. Willett, R. E. Butcher, C. P. Landee, and B. Twamley, Two halide exchange in copper(II) halide dimers: (4, 4'-bipyridinium) $\text{Cu}_2\text{Cl}_{6-x}\text{Br}_x$ , *Polyhedron* **25**, 2093 (2006).
- [74] Y. Ishii, G. Sala, M. B. Stone, V. O. Garlea, S. Calder, J. Chen, H. K. Yoshida, S. Fukuoka, J. Yan, C. dela Cruz, M.-H. Du, D. S. Parker, H. Zhang, C. D. Batista, K. Yamaura, and A. D. Christianson, Magnetic properties of the Shastry-Sutherland lattice material  $\text{BaNd}_2\text{ZnO}_5$ , *Phys. Rev. Mater.* **5**, 064418 (2021).
- [75] H. Lu, C. Xiao, R. Song, T. Li, A. E. Maughan, A. Levin, R. Brunecky, J. J. Berry, D. B. Mitzi, V. Blum, and M. C. Beard, Highly distorted chiral two-dimensional tin iodide perovskites for spin polarized charge transport, *J. Am. Chem. Soc.* **142**, 13030 (2020).